A TWO-FLUID, MHD CORONAL MODEL

S. T. Suess
NASA Marshall Space Flight Center, Huntsville, Alabama

A.-H. Wang, S. T. Wu
Dept. of Mech. Engineering and Center for Space Plasma and Aeronomic Research,
Univ. of Alabama, Huntsville, Alabama

G. Poletto
Osservatorio Astrofisico di Arcetri, Firenze, Italy

D. J. McComas
Los Alamos National Laboratory, Los Alamos, New Mexico

Short title:

Abstract. We describe first results from a numerical two-fluid MHD model of the global structure of the solar corona. The model is two-fluid in the sense that it accounts for the collisional energy exchange between protons and electrons. As in our single-fluid model, volumetric heat and momentum sources are required to produce high speed wind from coronal holes, low speed wind above streamers, and mass fluxes similar to the empirical solar wind. By specifying different proton and electron heating functions we obtain a high proton temperature in the coronal hole and a relatively low proton temperature in the streamer (in comparison with the electron temperature). This is consistent with inferences from SOHO/UVCS [*Feldman et al.*, 1977; *Kohl et al.*, 1997], and with the Ulysses/SWOOPS proton and electron temperature measurements which we show from the fast latitude scan. The density in the coronal hole between 2 solar radii and 5 solar radii ($2R_S$ and $5R_S$) is similar to the density reported from SPARTAN 201-01 measurements by *Fisher and Guhathakurta* [1994]. The proton mass flux scaled to 1 AU is $2.4 \times 10^8 cm^{-2}s^{-1}$, which is consistent with Ulysses observations [*Phillips et al.*, 1995]. Inside the closed field region, the density is sufficiently high so that the simulation gives equal proton and electron temperatures due to the high collision rate. In open field regions (in the coronal hole and above the streamer) the proton and electron temperatures differ by varying amounts. In the streamer, the temperature and density are similar to those reported empirically by *Li et al.* [1998] and the plasma β is larger than unity everywhere above $\sim 1.5\ R_S$, as it is in all other MHD coronal streamer models [e.g. *Steinolfson et al.*, 1982; *Gary and Alexander*, 1998].

1. Introduction

Sturrock and Hartle [1966] and *Hartle and Sturrock* [1968] were the first to show that the collisional energy exchange rate is too low to justify a single-fluid description of the solar wind. They gave a quantitative demonstration of this by analyzing the necessary condition, i.e. that the electron-proton collision frequency ν_E be substantially greater than the expansion rate ν_{exp} [*Spitzer*, 1962; *Braginskii*, 1965]. Outside a few solar radii the expansion rate may be estimated by the approximate expression:

$$\nu_{exp} \approx \frac{2v}{r} \tag{1}$$

where v is solar wind speed and r is heliocentric distance. The electron-proton collision frequency ν_E [*Braginskii*, 1965] is given by

$$\nu_E \approx 9 \times 10^{-2} n T_e^{-3/2} \tag{2}$$

where n is the number density of electrons (or protons) and T_e is the electron temperature. They estimated ν_{exp} and ν_E by using typical solar wind parameters at 1 AU to show that single-fluid theories of the solar wind are not adequate to describe the relative proton and electron temperatures. This early analysis appears to be essentially valid in light of all modern data. In spite of this, no published MHD global model incorporates two-fluid equations into a global description of the corona to demonstrate the transition between collisionally dominated coupling in streamers to collisional decoupling in coronal holes. With the advent of SOHO/UVCS, there is growing evidence that collisional effects are indeed important in the origin of slow solar wind and that the dominance of collisional processes differs between the edge and center of streamers [*Raymond et al.*, 1997; *Li et al.*, 1998]. *Raymond et al.* [1997] further find that streamers are surprisingly isothermal between the base of the streamer and $\sim 1.5\ R_S$. We describe here first results from a two-fluid model, showing that it can be used to analyze some of these problems and processes and reproduces such critical empirical results as a nearly

isothermal streamer. As in our one-fluid model [*Wang et al.*, 1998], volumetric heat and momentum sources are required to produce high speed wind from coronal holes, low speed wind above streamers, and mass fluxes similar to the empirical solar wind. The necessity for these source terms is easily understood since there is no explicit wave term in our equations and thus no explicit mechanism to produce high speed wind. Conversely, the physical mechanisms heating and accelerating the solar wind must produce the same consequences as our ad hoc source terms.

Although we only carry our calculation to 10 R_S, it is consistent with interplanetary observations of the mass flux as extrapolated back to the Sun. We show with Ulysses/SWOOPS data that it is also consistent with observations that the electron temperature is lower than the proton temperature in high speed wind and higher than the proton temperature in slow wind [see also *Burlaga and Ogilvie*, 1970, 1973; *Hundhausen et al.*, 1970; *Pizzo et al.*, 1973; *Formisano et al.*, 1974; *Neugebauer*, 1976; *Feldman et al.*, 1975, 1976; *Hundhausen*, 1972]. High speed wind comes from coronal holes [*Hundhausen*, 1972] and low speed wind somehow leaks from streamers [*Suess et al.*,1998; *Geiss et al.*, 1995; *Sheeley, et al.*, 1997; *Raymond et al.*, 1997]. Slow wind thus originates from a collisionally dominated part of the corona and fast wind comes from the nearly collisionless coronal holes. These conditions result in different temperatures and temperature histories as the solar wind expands from the Sun.

Our results can be compared with the many one-dimensional (1D) two-fluid models have been published since that of Hartle and Sturrock [*Hartle and Barnes*, 1970; *Whang*, 1972; *Hollweg*, 1973; *Esser, et al.*, 1986; *Habbal, et al.*, 1995; Hu et al., 1997]. These have been used to investigate detailed processes in solar wind heating and acceleration. In doing this, they generally deal with geometrical effects through a "spreading functions" [*Kopp and Holzer*, 1977; *Suess et al.*, 1998]. These models can serve to verify the correct solution has been found in our MHD model and to guide choices for the source terms, as was done for the terms used here and in *Wang et al.* [1998].

The evaluation of collisional effects in and around a streamer is one of the main reasons for our development of a two-fluid model and is motivated by results from SOHO/UVCS. In earlier models [*Wang et al.*, 1993; *Wang et al.*, 1995; *Suess et al.*, 1996; *Wang et al.*, 1998] the goal was determination of the boundary conditions and of heating and momentum sources which produce flow speeds and mass fluxes like those observed in both the fast and slow solar wind. We use those results here, obtaining a sharp cusp and low speed solar wind above streamers and high speed wind in coronal holes. This configuration, and the equivalent configuration in the absence of volumetric heating, lead to a natural transition between collisionally dominated plasma in the streamer and essentially collisionless plasma in the coronal hole. This transition is comparable with the transition described by *Raymond et al.* [1998] of the "first ionization potential" (FIP) dependence and the dependence of gravitational settling across streamers. They report that there is a difference between the core of the streamer, where the FIP effect is strongest, and the flanks of streamers (but, still inside streamers), where the FIP effect is less pronounced and more like that measured in slow solar wind. Although the mechanism by which slow solar wind leaks out of streamers is still not understood, the two-fluid model can be used to evaluate the coupling efficiency between the plasma components for comparison with the observations.

In section 2, the two-fluid global MHD equations are given and the numerical method and boundary conditions are described. Section 3 shows results from the numerical simulation and discusses the important physical processes. Conclusions and remarks are given in section 4.

2. Mathematical Description and Numerical Procedure

To preserve charge neutrality we assume equal electron and proton number densities and flow speeds. The MHD equations therefore have one continuity equation, one momentum equation, one induction equation, and two energy equations (one equation

each for electrons and protons). The model is axisymmetric, planar, and time-dependent with volumetric heating, momentum addition, and classical [*Spitzer*, 1962] thermal conduction. The governing equations in spherical polar coordinates can be written as follows:

$$\frac{\partial \rho}{\partial t} = -\frac{1}{r^2}\frac{\partial (r^2 \rho v_r)}{\partial r} - \frac{1}{r \sin\theta}\frac{\partial (\rho v_\theta sin\theta)}{\partial \theta} \tag{3}$$

$$\begin{aligned}\frac{\partial v_r}{\partial t} &= -v_r\frac{\partial v_r}{\partial r} - \frac{v_\theta}{r}\frac{\partial v_r}{\partial \theta} - \frac{1}{\rho}[\frac{\partial (\rho RT)}{\partial r} + \frac{{B_\theta}^2}{r} \\ &+ B_\theta(\frac{\partial B_\theta}{\partial r} - \frac{1}{r}\frac{\partial B_r}{\partial \theta})] + \frac{v_\theta^2}{r} - g(r) \\ &+ D(r,\theta)\end{aligned} \tag{4}$$

$$\begin{aligned}\frac{\partial v_\theta}{\partial t} &= -v_r\frac{\partial v_\theta}{\partial r} - \frac{v_\theta}{r}\frac{\partial v_\theta}{\partial \theta} - \frac{1}{\rho}[\frac{\partial (\rho RT)}{r\partial \theta} - \frac{B_r B_\theta}{\rho r} \\ &- B_r(\frac{\partial B_\theta}{\partial r} - \frac{1}{r}\frac{\partial B_r}{\partial \theta})] - \frac{v_r v_\theta}{r}\end{aligned} \tag{5}$$

$$\frac{\partial B_r}{\partial t} = \frac{1}{r \sin\theta}\frac{\partial}{\partial \theta}[sin\theta(v_r B_\theta - v_\theta B_r)] \tag{6}$$

$$\frac{\partial B_\theta}{\partial t} = -\frac{1}{r}\frac{\partial}{\partial r}[r(v_r B_\theta - v_\theta B_r)] \tag{7}$$

$$\begin{aligned}\frac{\partial T_e}{\partial t} &= -(\gamma - 1)[\frac{1}{r^2}\frac{\partial (r^2 v_r)}{\partial r} \\ &+ \frac{1}{r \sin\theta}\frac{\partial (v_\theta sin\theta)}{\partial \theta}]T_e + \nu_E(T_p - T_e) \\ &- v_r\frac{\partial T_e}{\partial r} - \frac{v_\theta}{r}\frac{\partial T_e}{\partial \theta} + \frac{\gamma - 1}{\rho R}Q_e \\ &- \frac{1}{\rho C_v}[\frac{1}{r^2}\frac{\partial (r^2 q_{er})}{\partial r} + \frac{1}{r \sin\theta}\frac{\partial (q_{e\theta} sin\theta)}{\partial \theta}]\end{aligned} \tag{8}$$

$$\begin{aligned}\frac{\partial T_p}{\partial t} &= -(\gamma - 1)[\frac{1}{r^2}\frac{\partial (r^2 v_r)}{\partial r} \\ &+ \frac{1}{r \sin\theta}\frac{\partial (v_\theta sin\theta)}{\partial \theta}]T_p + \nu_E(T_e - T_p) \\ &- v_r\frac{\partial T_p}{\partial r} - \frac{v_\theta}{r}\frac{\partial T_p}{\partial \theta} + \frac{\gamma - 1}{\rho R}Q_p \\ &- \frac{1}{\rho C_v}[\frac{1}{r^2}\frac{\partial (r^2 q_{pr})}{\partial r} + \frac{1}{r \sin\theta}\frac{\partial (q_{p\theta} sin\theta)}{\partial \theta}]\end{aligned} \tag{9}$$

$$p = \rho R(T_e + T_p) \tag{10}$$

where ρ is the plasma density ($\rho = nm_p$); T_e and T_p are the electron and proton temperatures, p is the isotropic pressure; v_r and v_θ are the flow velocities in the radial direction and meridional direction, B_r and B_θ are magnetic field intensities in the radial direction and meridional direction, C_v is the specific heat at constant volume for a monoatomic gas, γ (adiabatic index) is 5/3, and g is the gravitational acceleration. To further maintain higher proton temperatures in the coronal hole and higher electron temperatures in the streamer, Q_e and Q_p, volumetric heat sources are introduced for the electrons and protons, defined by

$$Q_e(r,\theta) = Q_0 \frac{\rho(r,\theta)}{\rho_0(\theta)}[1 + 0.25 \arctan(5(j-18))]e^{-0.1(r-R_S)/R_S} \tag{11}$$

$$Q_p(r,\theta) = Q_0 \frac{\rho(r,\theta)}{\rho_0(\theta)}[1 - 0.25 \arctan(5(j-18))]e^{-0.1(r-R_S)/R_S} \tag{12}$$

where Q_0 is 5×10^{-8} erg cm^{-3}s^{-1}, $\rho_0(\theta)$ is the base density, and j is the index of the grid point in the θ direction, running from 1 at a polar angle of -2.25^o to 22 at a polar angle of 92.25^o (i.e. $\theta = 4.5(j-1) - 2.25$ for j=1 to 22). These are similar to those used in by *Wang et al.* [1998] and although they depend on the density, equations (8) and (9) show these terms are divided by ρ so that the heating is effectively independent of the ambient medium. The heating term for electrons is larger near the equator than the pole while the heating term for the protons is larger near the pole than the equator. Also we assume that in the coronal hole ($\theta < 65.25^o$) and near the solar surface ($r < 2R_S$) the proton heating is zero since almost any proton heating near the base of the hole leads to excessive solar wind mass flux. The variation of these functions with polar angle are shown in Figure 1.

Finally, q_{er}, $q_{e\theta}$, q_{pr} and $q_{p\theta}$ are the radial and meridional thermal conduction fluxes for electrons and protons, which for a Lorentz gas are defined by,

$$\nabla \cdot \mathbf{q}_e = \nabla \cdot \left[\kappa_{e\|} T_e^{5/2} (\mathbf{B} \cdot \nabla T_e) \frac{\mathbf{B}}{B^2} \right] \tag{13}$$

$$\nabla \cdot \mathbf{q}_p = \nabla \cdot \left[\kappa_{p\|} T_p^{5/2} (\mathbf{B} \cdot \nabla T_p) \frac{\mathbf{B}}{B^2} \right] \tag{14}$$

where $\mathbf{B}$ is the magnetic field vector, and $\kappa_{e\|}$ and $\kappa_{p\|}$ are the collisional thermal conductivities along the magnetic field lines for electrons and protons, respectively, and given by *Spitzer*[1962]. D is the momentum source term, defined as in *Wang et al.* [1998] to be:

$$D(r,\theta) = \frac{D_0 a^2}{(r-a)^2 + a^2}\{1 - 0.25\arctan[5(j-16)]\} \tag{15}$$

where $D_0 = 5 \times 10^3$ dyn/g and $j(\theta)$ is defined the same as in equations (11) and (12). This produces solar wind speeds similar to empirical values [*Phillips, et al.*, 1995]. We assume the momentum source is time-stationary, does not depend on ambient plasma properties, and that it increases in the lower corona and then decreases more rapidly than the heating term above $7R_S$. The position of the maximum value of $D(r,\theta)$ is at $a = 3.5R_S$. A detailed discussion of this term is given by *Wang et al.* [1998]. Since the deposition height of $D(r,\theta)$ affects the high speed wind proton mass flux [*Leer and Holzer*, 1980; *Wang et al.*, 1998] we have also set $D(r,\theta)$ equal to zero inside $2R_S$ for $0 \leq \theta \leq 65.25^o$ (i.e., in the coronal hole), thereby avoiding excessive proton mass flux in the high speed wind.

There is no physics behind the Q and D source terms. They are based solely on empirical requirements and the formalism used in earlier models of our own and others, although some aspects of the functions can be rationalized on a physical basis. For example, taking $Q_p > Q_e$ in the coronal holes can be justified by the fact that waves are observed in the high speed wind and many waves (e.g. ion-cyclotron waves) dissipate in the heavier particles. That $Q_e \neq 0$ in the coronal holes derives only from the empirical requirement to avoid a too small T_e [*Tu and Marsch*, 1997]. There is no obvious explanation for preferential heating of electrons above streamers, but this is also an empirical requirement.

The computational domain is in a meridional quadrant from the pole to the equator in θ and from the solar surface to $10R_S$ in the radial direction. The numerical scheme and the boundary conditions are described by *Wu and Wang* [1987], *Wang et al.* [1993]

and *Suess et al.* [1996]. The only difference here is that at the lower boundary, after the total temperature of electrons and protons is calculated from the characteristic equations, we specify either the electron temperature or the proton temperature to obtain the other temperature from the total temperature. This is because in the characteristic equations the proton temperature and the electron temperature are dependent on each other. In the present simulation the electron temperature is fixed at the lower boundary during the computation.

3. Simulation Results and Discussion

To test the two-fluid model, we first reproduced the one dimensional two-fluid model of *Hartle and Sturrock* [1968] by deleting the heating and momentum sources and making the computation only in the radial direction. Then, similar to previous solar minimum type coronal simulations, we chose an initial ($t = 0$) state with a dipole potential magnetic field and an expanding atmosphere. In the initial expanding atmosphere, $T(r,\theta)$ and $T_p(r,\theta)$ are initially defined everywhere somewhat arbitrarily, but guided by empirical results. Then, $T_e(r,\theta) = T(r,\theta) - T_p(r,\theta)$ and the momentum equation is solved for $v_r(r,\theta)$. This is done separately along each value of θ on the grid. Thus, the $t = 0$ density, temperature and radial velocity depend on latitude as well as radius. All other parameters are identical to those used by *Wang et al.* [1998]. The density at the last meridional grid point before the equator (87.75°) on the solar surface is $1.26 \times 10^8\,\mathrm{cm}^{-3}$. The proton and electron temperatures are 2.15×10^6 K and 1.74×10^6 K, respectively, at the same position. The magnetic field intensity at that point is 1.24 gauss, giving a plasma β of ~0.5. The initial conditions for the flow variables are shown in Figure 2. This shows that the base density and electron temperature are higher in the streamer and the proton temperature is lower in the streamer. These differences generally persist throughout the relaxation, as determined by the compatibility relations at the boundary [*Wang et al.*, 1998]. However, the flow speed changes both at the base

and throughout the computational volume, eventually becoming very small in the core of the streamer, and $T_e \sim T_p$ at the base for all θ.

The system relaxes to a quasi-steady state after 20 hours in physical time, which is long enough to complete the rapid relaxation phase out to the distance of $\sim 10\ R_S$ [*Steinolfson, Suess, and Wu*, 1982; *Suess et al.*, 1996]. At larger times, the streamer continues to slowly leak plasma due to the heating near the top of the streamer, where even without heating $\beta >> 1$. This occurs because the heating increases the temperature at the top of the streamer until plasma pressure slowly forces open additional field lines in a process which we call " streamer evaporation." An eventual equilibrium exists because thermal conduction constitutes a heat sink at the base, but this only occurs after months of time in the present simulation. Evaporation is therefore a limited process which produces slow solar wind and slowly reduces the height of the streamer [*Suess et al.*, 1996]. Heating and momentum sources that depend more strongly on physical parameters or are confined to very low heights in the streamer may lead to sporadic releases of slow wind and reclosing of the high streamer, as reported by *Sheeley et al.* [1997].

The physical configuration of the magnetic field in the corona after t=20 hours is shown in Figure 3, where it is seen that the topology is virtually identical to that found in the one fluid model [*Wang et al.*, 1998]. This is not surprising, since the topology is dominated by the MHD interaction between the bulk plasma density and the magnetic field, and should be essentially independent of whether a two-fluid model is used. A qualification to this might be if the plasma became collisionless in the streamer which could lead to a difference in thermal pressure relative to a one-fluid model. But electron-proton decoupling occurs only in the coronal hole at some height above the base and therefore has little influence on the detailed topology of the streamer. In the following, all the dependent variables are referenced to the time of 20 hours after the relaxation begins.

The density and radial velocity versus polar angle at several radial positions are shown in Figure 4. From this figure, we notice some differences between the two-fluid model and the one-fluid model, which result mainly from setting the momentum source to zero low in the coronal hole and from slightly different boundary conditions. Specifically, in the coronal hole the two-fluid density decreases faster and the radial velocity is lower than in the single-fluid model [*Wang, et al.*, 1998]. In the present simulation, the density falls from $\sim 2.0 \times 10^7\ cm^{-3}$ at $1R_S$ to $10^4\ cm^{-3}$ at $5.27R_S$. The radial velocity is $5km/s$ at $1R_S$ and $455km/s$ at $5.27R_S$. The proton mass flux in the coronal hole, also at $5.27R_S$, but scaled to 1 AU, is $\sim 2.4 \times 10^8\ cm^{-2}s^{-1}$. This is consistent with Ulysses measurements [*Phillips et al.*, 1995].

Figure 5 shows a comparison of the model with various observations of the radial variation of density between $2R_S$ and $5R_S$ in coronal holes. The two solid lines are from the present model, the dot-dashed line is from SPARTAN 201 [*Fisher and Guhathakurta*, 1994], the dotted line is from *Newkirk* [1967], and the dashed line is from *Munro and Jackson* [1977]. The model density in the coronal hole is almost identical with density from SPARTAN 201. This agreement is largely dependent on the combination of boundary conditions and choices for the heating and momentum sources. Other combinations may provide an equally good agreement but it is not easy to carry out a comprehensive survey of parameter space. Instead, we expect in the future to try other combinations based on physical arguments.

The most important result from the two-fluid model is what it predicts for temperatures as a consequence of collisional energy exchange. Since the energy exchange rate between electrons and protons is very low almost everywhere in the corona except in the dense closed field lines region, it is of interest to examine how thermal conduction and collisions affect the two species. Figure 6 shows the distribution of the electron and proton temperatures at various heights. The solid line is the electron temperature and the dotted line is the proton temperature. This should be viewed in comparison with

Figure 1, which is a plot of the distribution of heating rates for electrons and protons versus polar angle. Also in Figure 6 the data has been folded over to simulated both hemispheres. This will facilitate the comparison below with Ulysses measurements.

The lowest level shown in Figure 6 is 1.16 R_S, which is the third grid point above the boundary in the simulation. This curve shows that everywhere in the low corona the collision rate is high enough to closely couple T_e and T_p, in spite of differing heating functions for protons and electrons. Above this level, the proton temperature is higher than the electron temperature in the coronal hole due to the higher proton heating rate and low collision rate. Inside the closed field in the streamer, up to $\sim 5.0 R_S$, the high density and resultant high collision rate cause the electron temperature to be almost the same as the proton temperature. The electron temperature then becomes larger than the proton temperature above the streamer where the collision rate has fallen and the electron heating is still greater than the proton heating.

Observationally, there is now beginning to be some evidence on the relative values of proton and electron temperature from SOHO/UVCS line widths [*Kohl et al.*, 1997] although more detailed analysis and some modeling will be required for accurate empirical temperature estimates. What has been reported so far is that in coronal holes UVCS protons have "kinetic temperatures" of several million degrees while some heavier ions have kinetic temperatures of tens or even hundreds of millions of degrees. These temperatures are believed to reflect waves and the kinetic temperature is highly anisotropic, being lower in the radial direction. Nevertheless, indications are that the proton temperature in coronal holes is higher than the electron temperature at $\sim$ 2 R_S. In addition, T_p may increase between $1.5 R_S$ and $3.0 R_S$. Comparison between these observations and our model is necessarily very limited since the model does not explicitly include waves and therefore does not compute the kinetic temperature. We could nevertheless probably force T_p to increase between 1.5 and $2.0 R_S$ by increasing the amplitude while shortening the scale height of Q_p because of the absence of heating

below $2.0 R_S$. In streamers, the kinetic temperature is more nearly isotropic and there appears to be a less intense wave contribution so that the comparisons with our model are more viable there. At heliocentric heights of 1.5 R_S in equatorial streamers the results from UVCS are consistent with a thermal distribution at about 2×10^6 K.

UVCS results from coronal holes have stimulated the development of several 1D corona flow models incorporating $T_p > T_e$. One such model is that by *Hu et al.* [1997] which includes the effects of temperature anisotropies. It features generally higher T_p than T_e, although below 2.0 R_S, $T_e > T_p$. Therefore, it differs from our results in detail. Such models demonstrate how electrons carry the conduction heat flux in the high speed wind and show heating is required to keep their temperature relatively high far out into the interplanetary medium [see also *Tu and Marsch*, 1997]. Conversely, protons cool nearly adiabatically in the high speed wind. This also occurs for the temperatures above the coronal hole in our model since the electrons and protons are essentially collisionless at this height.

There is very good data on interplanetary proton and electron relative and absolute temperature variations from Ulysses, showing that $T_p > T_e$ in the high speed wind and that $T_e > T_p$ in slow wind. Figure 7 shows Ulysses/SWOOPS measurements during the fast latitude scan [*Phillips et al.*, 1995], which was the one-year period from September 1994 to July 1995 during which Ulysses swept from 80° S heliographic latitude to 80° N heliographic latitude. This was effectively at solar sunspot minimum so the corona was well approximated by the dipole field used in the present simulation. The plotted temperatures are one-hour averages. Both the electron and proton data were first sorted by magnitude and the top 2% were dropped to eliminate the outlying data values that are all due to evaluation of poorly determined distribution functions. What is left is an accurate illustration of the actual variance in the temperature data - there is a great deal of variability from one hour to the next. The figure shows the previously described relative variation of the electron and proton temperatures in high and low speed wind.

Plotting the one-hour averages also clearly displays the sharp temperature boundary at the edge of the high speed flow that is the counterpart of the sharp boundary in flow speed [*McComas et al.*, 1998]. The temperatures are plotted as measured, with no adjustment for distance from the Sun, so the apparent latitudinal gradient in temperature is an illusion of orbital motion rather than a measurement of a real variation across the coronal hole. Ulysses ranges from less than 1.4 AU at the equator (perihelion) to more than 2.0 AU at 80° latitude. There are also systematic variations across the coronal holes, but they are much smaller than the variation shown here due to the changing radius of Ulysses. Although we have not attempted to extrapolate these temperatures back to the Sun, they have the approximate relative values and absolute magnitudes that would be expected from the temperatures at 10 R_S shown in Figure 6. This result was not imposed a priori on the model. Rather, it is a consequence of fitting the mass flux, coronal temperatures, and flow speeds.

Our two-fluid model simulates the empirical results by using a higher proton than electron heating rate in the coronal hole and a lower rate in the streamer. For the same amount of heating of protons in the coronal hole and the electrons in the streamer, $T_p > T_e$ in the hole while T_e is comparable to, but slightly larger than T_p in the streamer. This is because in the coronal hole the density is low so the collision rate is low as well and while the protons gain energy from the heat source, they give little to the electrons. In the streamer the densities and collision rates are higher. Thus, the electrons gain energy from the heat source but also transfer some of that energy to the protons. A consequence of this is the shift with height of the latitude at which $T_e = T_p$. This point is used to label the curves in Figure 6, and it clearly moves towards the equator with increasing height. This is not the same as the width of the streamer because the source terms and boundary conditions are not physically tied to the streamer geometry in this simulation. Tying the streamer width, source terms, and boundary conditions more closely together will be a topic of future work.

The electron-proton temperature difference is displayed in Figure 8 as a function of heliocentric distance, at three different polar angles. The purpose of this figure is to show that these differences become nearly independent of radius at the pole and equator. Since both temperatures decrease with radius, the relative differences will increase with radius. This plot illustrates something which is not easily seen in Figure 6; this is that the absolute temperature difference in the streamer is several tens of thousands of degrees, which is masked by the higher absolute temperature in the streamer. The heating terms are negligible near the outer boundary of the computational domain so it can be anticipated that carrying the computation to larger radii would show the proton temperature decreasing ~adiabatically and the electron temperature decreasing more slowly.

Figure 7 also illustrates that considerable work needs to be done in more closely associating the source functions with the geometry, here in simulating the sharp boundary between the high and low speed wind. The present model, with boundary conditions varying slowly in latitude and source functions that do not depend on the ambient plasma and magnetic field properties, gives a gradual transition from high speed to slow wind. Empirically, the boundary between high and low speed flow is sharp, well defined, and distinct even at large distances from the Sun [*McComas et al.*, 1998]. The detailed results on this boundary from the Ulysses fast latitude scan provides ample material to help guide analysis of the conditions in the corona that are required to produce the interplanetary signature. This is further known to be a boundary which exists through the corona and down to the photosphere [*Geiss et al.*, 1995]. A model simulating these properties would be much better for also simulating CMEs since the propagation characteristics of CMEs across the boundaries of steamers and into coronal holes depends strongly on the ambient characteristic wave speeds [*Steinolfson*, 1988].

4. Conclusions and Discussion

The two-fluid MHD coronal model described here has been used to analyze the efficiency of collision rates in coronal holes and streamers to see if the model is consistent with solar wind and coronal observations. Since the bulk transfer of momentum and energy is similar to that in a one-fluid model, the configuration, flow speeds, and densities are essentially like those in the one-fluid model. This is also reflected in the values of the plasma β in the model, which are much smaller than unity in the coronal hole and larger than unity in the streamer above $\sim$ 1.3 R_S. The flow properties are what would be expected from solar wind observations [*Phillips et al.*, 1995] and the plasma β is compatible with empirical estimates in coronal holes [*Suess and Smith*, 1996] and in streamers [*Li et al.*, 1998].

However, the two-fluid model is also able to show the decoupling of electrons and protons as slow wind moves away from the Sun above streamers. It also exhibits the anticipated property that electrons and protons are only very weakly coupled in the high speed flow in coronal holes, allowing them to maintain different temperatures and completely different temperature histories.

However, the model has a considerably greater utility than simply evaluating collision rates. With the additional information on electron and proton temperatures in coronal holes, in the cores of streamers, in the flanks of streamers, and in the high and low speed solar wind, this becomes a tool for analyzing the transfer of energy and momentum to the solar wind, the acceleration of the high speed solar wind, and the origin of the slow solar wind. For example, *Raymond et al.* [1997, 1998] and *Li et al.* [1998] report that the FIP effect differs between the core and flanks of streamers and is absent outside the bright boundary of streamers. The FIP effect in the flanks of streamers is like that in slow wind, while that in the core is greater than the slow wind and suggests complete gravitational settling. This in turn suggests that the wind on flanks of streamers is not steady, but rather is disturbed on a time scale comparable to

the few-day gravitational settling time. Sporadic releases of (slow) solar wind from the streamers, as reported by *Sheeley et al.* [1997] could account for this if they came from the flanks. The evaporation of the streamer that exists in this and our earlier models with volumetric heating, produces such an effect, and other choices for heating and momentum sources can lead to sporadic, episodic releases of mass from the streamers instead of the more gradual evaporation that is described here.

The model also contains a signature of the acceleration of the fast solar wind. The relative temperatures of the electrons and protons in the solar wind is an indirect indication of the heating and acceleration. But, when combined with information on the temperatures in coronal holes, a stronger constraint is placed on sources. It is important to remember that the solution presented here is not unique. Other combinations of boundary conditions, and the radial and meridional dependences of the source functions will produce similar results at 1 AU or 10 R_S. The sources described in (11), (12), and (15) contain heating to quite large distances from the Sun and the momentum source does not depend in any way on the ambient plasma conditions. Utilizing information on coronal hole temperatures will probably require modifying or relaxing the restrictive assumptions used in (11), (12), and (15).

Remnant signatures of coronal processes are also contained in the solar wind plasma distribution functions, and these depend on collision rates in the corona. The most well known of these is the electron "strahl" that is an excess electron ($\geq$ 100 eV) halo component of the solar wind most closely aligned with the magnetic field. Strahl-associated suprathermal electrons originate in the inner corona and move freely out to 1 AU, providing information on the state of the corona [*Fitzenreiter, et al.*, 1998]. The strahl is strongest and narrowest in high speed wind, becoming wider when the speed is low. The presence of the strahl in high speed wind depends on the history of the flow, in addition to conditions in the corona. The present two-fluid results are probably consistent with the strahl observations because the decoupling of electrons

and protons in the coronal hole might allow the suprathermal particles to escape, while collisions between electrons and protons remove the possibility of a strahl forming above streamers. But it would require detailed analysis to show that a strahl could exist in the modeled slow wind.

In the future, this model will also be used to simulate coronal mass ejections (CMEs). This will permit studies of collisional processes in determining abundance anomalies in CMEs. However, there remains a great deal to be done in analyzing quasi-steady flow in order to determine: (a) the properties of streamers and their stability or meta-stability under varying types of heating, and (b) the relative values of T_p and T_e at various levels in coronal holes for comparison with UVCS and other SOHO instrument observations.

Acknowledgments.

S. Suess has been supported by the Ulysses/SWOOPS and SOHO/UVCS projects of NASA. The work of G. Poletto has been partially supported by ASI (Italian Space Agency). A.-H. Wang and S. T. Wu have been supported by the Naval Research Laboratory through USRA N00014-C-95-2058, by NSF grant ATM9633629, and by NASA grant NAG AW-4665. The work of D. McComas was carried out under the auspices of the US Department of Energy with support from NASA under the Ulysses project.

References

Braginskii, S. I., Transport processes in a plasma, in *Reviews of Plasma Physics* (M. A. Leontovich, ed.), vol. 1, pp. 205-311, Consultants Bureau, New York, 1965.

Burlaga, L. F. and K. W. Ogilvie, Heating of the solar wind, *Astrophys. J., 159*, 659-670, 1970.

Burlaga, L. F. and K. W. Ogilvie, Solar wind temperature and speed, *J. Geophys. Res., 78*, 2028-2034, 1973.

Esser, R., E. Leer, S. R. Habbal and G. L. Withbroe, A two-fluid solar wind model with Alfvén waves: parameter study and application to observations, *J. Geophys. Res., 91*, 2950, 1986.

Feldman, W. C., J. R. Asbridge, S. J. Bame and J. T. Gosling, Plasma and magnetic fields from the sun; high speed solar wind flow parameters at 1 AU, *J. Geophys. Res., 81*, 5054, 1976.

Feldman, W. C., J. R. Asbridge, S. J. Bame and J. T. Gosling, Plasma and magnetic fields from the Sun, *The Solar Output and Its Variations* (O. R. White, ed.), p. 351, Colorado Associated University Press, Boulder, 1977.

Feldman, W. C., J. R. Asbridge, S. J. Bame and M. D. Montgomery and S. P. Gary, Solar wind electrons, *J. Geophys. Res., 80*, 4181-4196, 1975.

Fisher, R. R., and M. Guhathakurta, SPARTAN 201 White Light Coronagraph experiment, *Space Sci. Rev., 70*, 267, 1994.

Fitzenreiter, R. J., K. W. Ogilvie, D. J. Chornay, and J. Keller, Observations of electron velocityh distribution functions in the solar wind by the WIND spacecraft: High angular resolution strahl measurements, *Geophys. Res. Lett., 25(3)*, 249-252, 1998.

Formisano, V., G. Moreno and E. Amata, Relationships among the interplanetary plasma parameters: Heos 1, Decembr 1968 to December 1969, *J. Geophys. Res., 79*, 5109-5117, 1974.

Gary, G. A., and D. Alexander, Constructing the coronal magnetic field, *Sol. Phys.*, submitted, 1998.

Geiss, G., G. Gloeckler, R. von Steiger, H. Balsiger, L. A. Fisk, A. B. Galvin, F. M. Ipavich, S. Livi, J. F. McKenzie, K. W. Ogilvie, and B. Wilken, The southern high speed stream: Results from the SWICS instrument on Ulysses, *Science, 268*, 1033, 1995.

Habbal, S. R., R. Esser, M. Guhathakurta, and R. R. Fisher, Flow properties of the solar wind derived from a two-fluid model with constraints from white light and in situ interplanetary observations, *Geophys. Res. Lett., 22*, 1465, 1995.

Hartle, R. E., and A. Barnes, Nonthermal heating in the two-fluid solar wind model, *J. Geophys. Res., 75*, 6915, 1970.

Hartle, R. E., and P. A. Sturrock, Two-fluid model of the solar wind, *Astrophys. J., 151*, 1155, 1968.

Hollweg, J. V., Alfvén waves in a two-fluid model of the solar wind, *Astrophys. J., 181*, 547, 1973.

Hu, Y.-Q., R. Esser, and S. R. Habbal, A fast solar wind model with anisotropic proton temperature, *J. Geophys. Res., 102*, 14,661, 1997.

Hundhausen, A. J., S. J. Bame, J. R. Asbridge and S. J. Sydoriak, Solar wind proton, properties: Vela 3 observations from July 1965 to June 1967, *J. Geophys. Res., 75*, 4643, 1970.

Hundhausen, A. J., *Coronal Expansion and Solar Wind*, Springer-Verlag, New York, 1972.

Kohl, J., and 25 others, First Results from the SOHO Ultraviolet Coronagraph Spectrometer, *Solar Phys, 175(2),* 613-644, 1997.

Kopp, R. A., and T. E. Holzer, Dynamics of coronal hole regions I. Steady polytropic flows with multiple critical points, *Solar Phys., 49,* 43-56, 1977.

Leer, E., and T. E. Holzer, Energy addition in the solar wind, *J. Geophys. Res., 85*, 4681, 1980.

Li, J., J. C. Raymond, L. W. Acton, J. Kohl, M. Romoli, G. Noci, and G. Naletto, Physical structure of a coronal streamer in the closed field region observed from UVCS/SOHO and SXT/Yohkoh, *Astrophys. J.*, in press, 1998.

McComas, D. J., P. Riley, J. T. Gosling, A. Balogh, and R. Forsyth, Ulysses' rapid crossing of the polar coronal hole boundary, *J. Geophys. Res., 103*, 1955-1967, 1998.

Munro, R. H., and B. V. Jackson, Physical properties of a polar coronal hole from 2 to $5R_S$, *Astrophys. J., 213*, 874, 1977.

Neugebauer, M., The quiet solar wind, *J. Geophys. Res., 81*, 4664-4670, 1976.

Newkirk, G. A., Jr., Structure of the solar corona, *Ann. Rev. Astron. Astrophys., 5*, 213, 1967.

Phillips, J. L., et al., Ulysses solar wind plasma observations from pole to pole, *Geophys. Res. Lett., 22*, 3301, 1995.

Pizzo, V., J. T. Gosling, A. J. Hundhausen and S. J. Bame, Large-scale dynamical effects upon the solar wind flow parameters, *J. Geophys. Res., 78*, 6469, 1973.

Raymond, J. C., J. L. Kohl, G. Noci, and 24 others, Composition of coronal streamers from the SOHO Ultraviolet Coronagraph Spectromoter, *Sol. Phys., 175(2)*, 646-655, 1997.

Raymond, J., R. Suleiman, A. van Ballegooijen, and J. Kohl, Absolute abundances in streamers from UVCS, in "Correlated Phenomena at the Sun, in the Heliosphere, and in Geospace," Proc. of 31st ESLAB Symposium (B. Fleck, ed.), ESA publ. SP-415, in press, 1998.

Sheeley, N. R., Y.-M. Wang, S. H. Hawley, G. E. Brueckner, K. P. Dere, R. A. Howard, M. J. Koomen, C. M. Korendyke, D. J. Michels, S. E. Paswaters, D. G. Socker, O. C. St. Cyr, D. Wang, P. L. Lamy, A. Llebaria, R. Schwenn, G. M. Simnett, S. Plunkett, and D. A. Biesecker, Measuerements of flow speeds in the corona between 2 and 30 $R_\odot$, *Astrophys. J., 484*, 472, 1997.

Spitzer, L., *Physics of Fully Ionized Gases.* 2nd rev. ed., John Wiley, New York, 1962.

Steinolfson, R. S., S. T. Suess, and S. T. Wu, The steady global corona, *Astrophys. J., 255*, 730-742, 1982.

Steinolfson, R. S., Density and white light brightness in looplike coronal mass ejections: Importance of the preevent atmosphere, *J. Geophys. Res., 83*, 14,251, 1988.

Sturrock, P. A., and R. E. Hartle, Two-fluid model of the solar wind, *Phys. Rev. Lett., 16*, 628, 1966.

Suess, S. T., A. H. Wang, and S. T. Wu, Volumetric heating in coronal streamers, *J. Geophys. Res., 101*, 19957, 1996.

Suess, S. T., J. L. Phillips, D. J. McComas, B. E. Goldstein, M. Neugebauer, and S. Nerney,

The solar wind - inner heliosphere, *Adv. in Spa. Res.*, in press, 1998.

Suess, S. T., A.-H. Wang, S. T. Wu, and G. Poletto, The geometric spreading of coronal plumes and coronal holes, *Solar Phys.*, in press, 1998.

Suess, S. T., and E. J. Smith, Latitudinal dependence of the radial IMF component: Coronal imprint, *Geophys. Res. Lett., 23(22)*, 3267-3270, 1996.

Tu, C.-Y., and E. Marsch, Two-fluid model for heating of solar corona and acceleration of the solar wind by high-frequency Alfvén waves, *Solar Phys., 171*, 363-391, 1997.

Wang, A. H., S. T. Wu, S. T. Suess, and G. Poletto, A two-dimensional MHD global coronal model: Steady-state streamers, *Sol. Phys., 147*, 55, 1993.

Wang, A. H., S. T. Wu, S. T. Suess, and G. Poletto, Numerical Modeling of coronal mass ejections based on various preevent model atmospheres, *Sol. Phys., 161*, 365, 1995.

Wang, A. H., S. T. Wu, S. T. Suess, and G. Poletto, Global model of the corona with heat and momentum addition, *J. Geophys. Res., 103*, 1913, 1998.

Whang, Y. C., A solar-wind model including proton thermal anisotropy, *Astrophys. J., 178*, 221, 1972.

Wu, S. T., and J. F. Wang, Numerical tests of a modified full implicit, continuous, Eulerian (FICE) scheme with projected characteristic boundary conditions for MHD flow, *Comput. Methods Appl. Mech. Eng., 64*, 267, 1987.

S. T. Suess, NASA Marshall Space Flight Center, ES82, Huntsville, AL 35812. (email: steve.suess@msfc.nasa.gov)

A.-H. Wang and S. T. Wu, Dept. of Mech. Engineering and Center for Space Plasma and Aeronomic Research, Univ. of Alabama, Huntsville, AL 35899. (email: wanga@cspar.uah.edu, wu@cspar.uah.edu)

G. Poletto, Osservatorio Astrofisico di Arcetri, Largo Enrico Fermi, 5, 50125 Firenze, Italy (email poletto@arcetri.astro.it)

D. J. McComas, Los Alamos National Laboratory, D466, Los Alamos, NM 87545. (email mccomas@nis-pop.lanl.gov)

Received _____

Submitted *Journal of Geophysical Research*, 1998.

Figure 1. The meridional dependence at $r = R_S$ of the electron and proton volumetric heating functions, as given by equations (11) and (12). The proton heating function, (12), is further modified in the simulation to be zero poleward of 62.5^o and inside 2 R_S to restrict the mass flux from becoming larger than observed in the solar wind.

Figure 2. Temperature, density, and flow speed in the initial ($t = 0$) state. The electron temperature is shown as a solid line and the proton temperature is shown as a dashed line.

Figure 3. Magnetic field line topology in the simulation after a relaxation time of 20 hours physical time. This time is long compared to the rapid relaxation phase inside 10 R_S [*Suess et al.*, 1996]. Beyond this time the solution is quasi-steady, with slow evaporation from the top of the streamer. The topology is like that for the one-fluid model as one would expect.

Figure 4. Density and radial flow speed versus polar angle in the simulation, at the same physical time of 20 hours as in Figure 3.

Figure 5. Density versus height, between 2.0 and 5.0 R_S. The two solid lines are the model densities at the pole and the equator. This is compared to three measurements made in coronal holes: the dot-dashed line is from SPARTAN 201-01 [*Fisher and Guhathkurta*, 1994], the dotted line is from *Newkirk* [1967], and the dashed line is from *Munro and Jackson* [1977].

Figure 6. Proton and electron temperatures from the simulation, versus polar angle at several heights between 1.0 and 10.4 R_S. The proton temperatures are the dotted lines and the electron temperatures are the solid lines. The radius for each pair of lines is indicated at the intersection of that pair (e.g. the top two curves are at 1.0 R_S). The curves have been reflected at the equator, showing the opposite hemisphere, to facilitate comparison with the Ulysses data shown in Figure 7.

Figure 7. Electron and proton temperature data from Ulysses/SWOOPS (the Ulysses solar wind plasma instrument) during the fast latitude scan between September 1994 and July 1995. One-hour averages of the temperatures are plotted versus heliographic latitude, with the highest 2% of both the electron and proton values being dropped due to their resulting from poorly determined plasma distribution functions. The values are not scaled with radius.

Figure 8. The electron-proton temperature difference, $T_e - T_p$, versus radius, at three different constant polar angles.

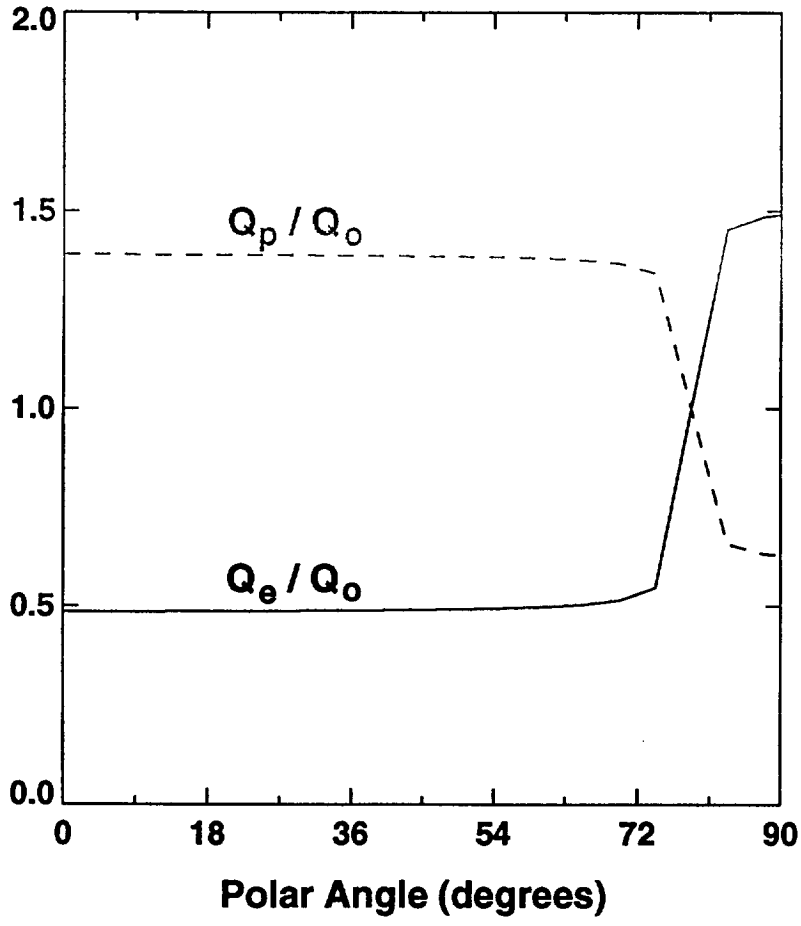

Figure 1
A Two-Fluid MHD Coronal Model
Suess, Wang, Wu, Poletto, & McComas

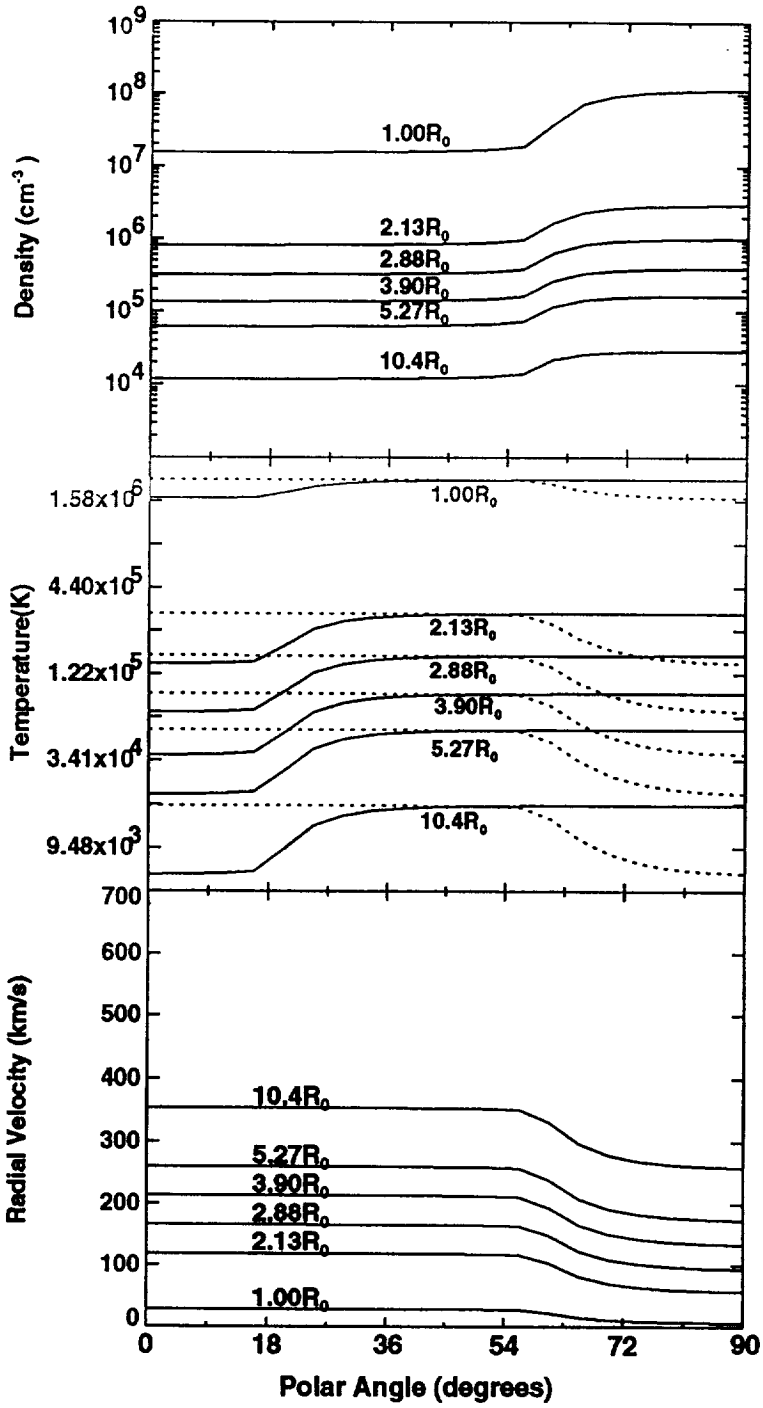

Figure 2
A Two-Fluid MHD Coronal Model
Suess, Wang, Wu, Poletto, & McComas

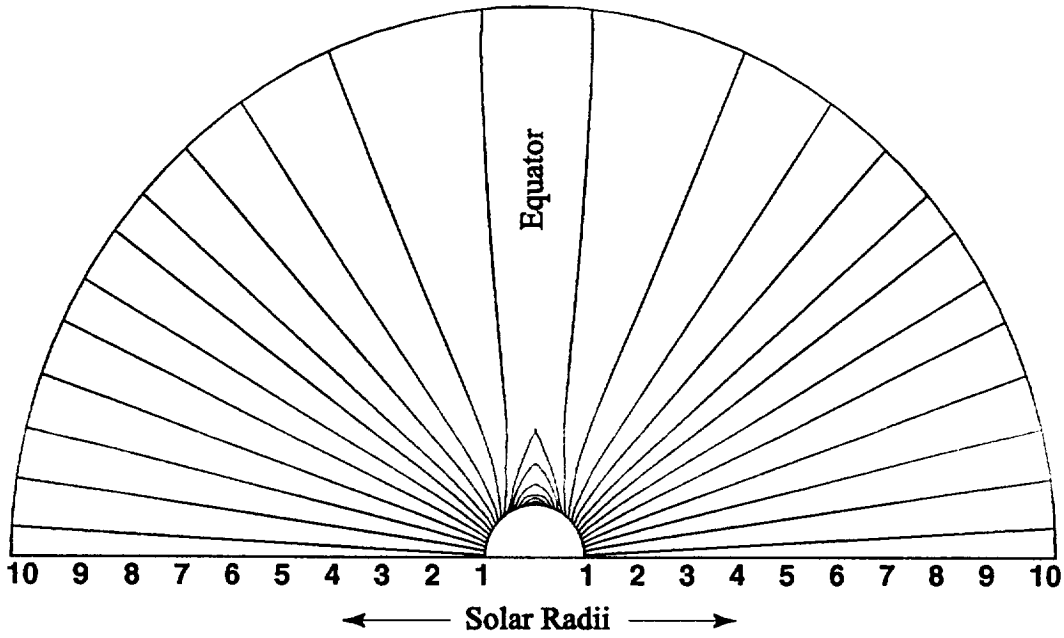

Figure 3–
A Two-Fluid MHD Coronal Model
Suess, Wang, Wu, Poletto, & McComas

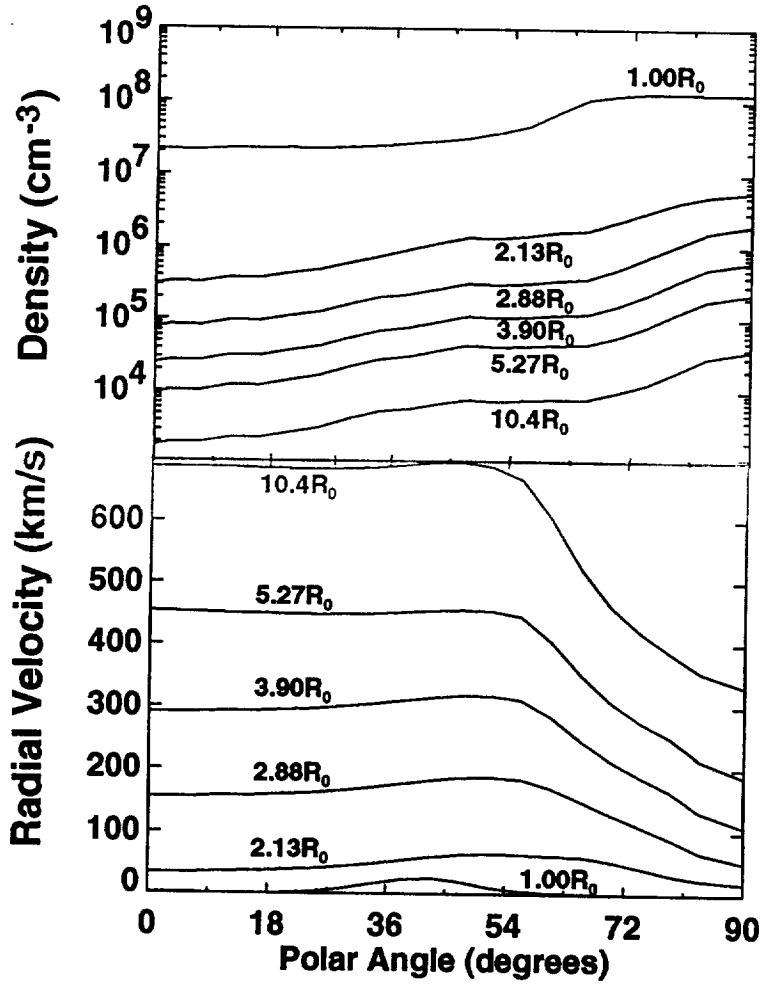

Figure 4
A Two-Fluid MHD Coronal Model
Suess, Wang, Wu, Poletto, & McComas

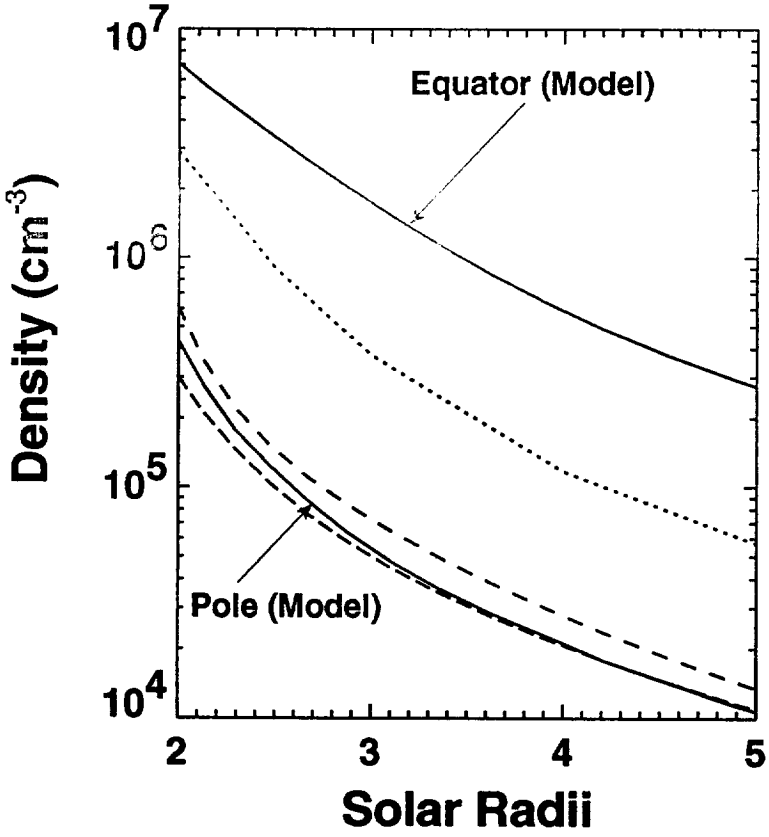

Figure 5–
A Two-Fluid MHD Coronal Model
Suess, Wang, Wu, Poletto, & McComas

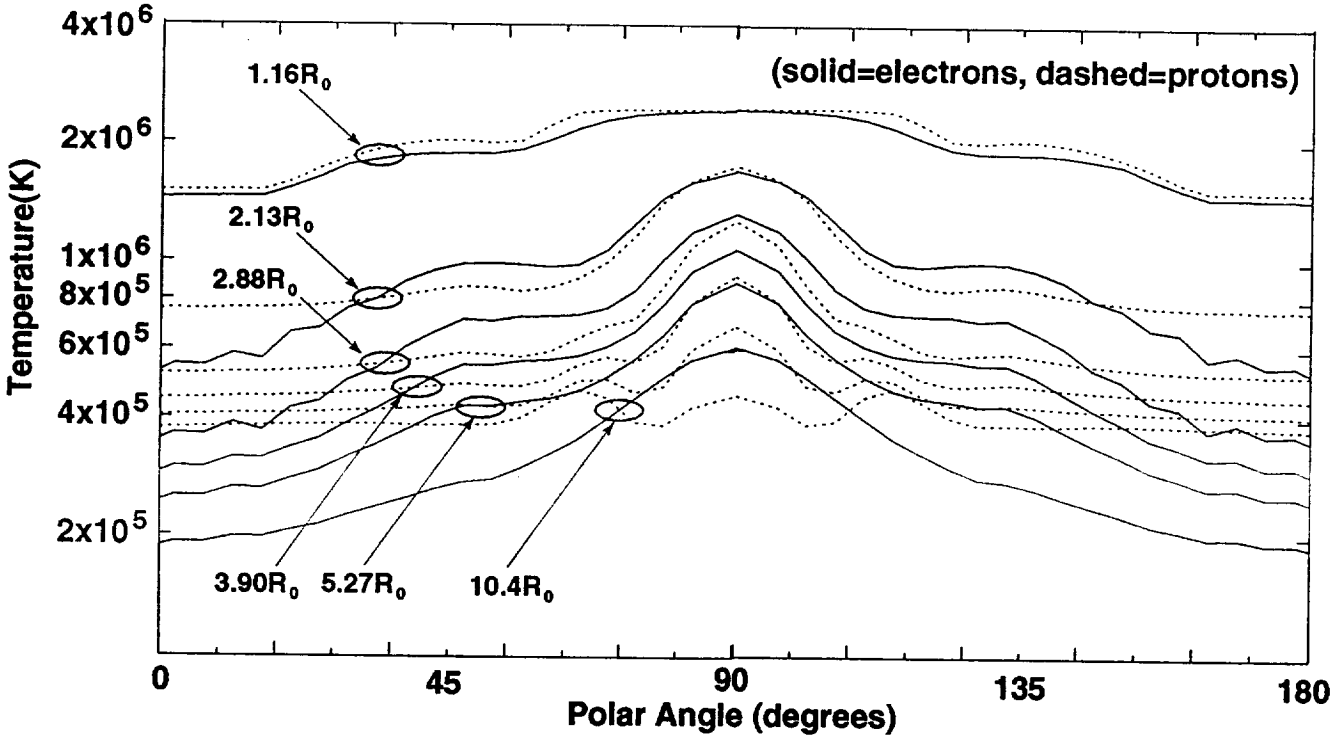

Figure 6
A Two-Fluid MHD Coronal Model
Suess, Wang, Wu, Poletto, & McComas

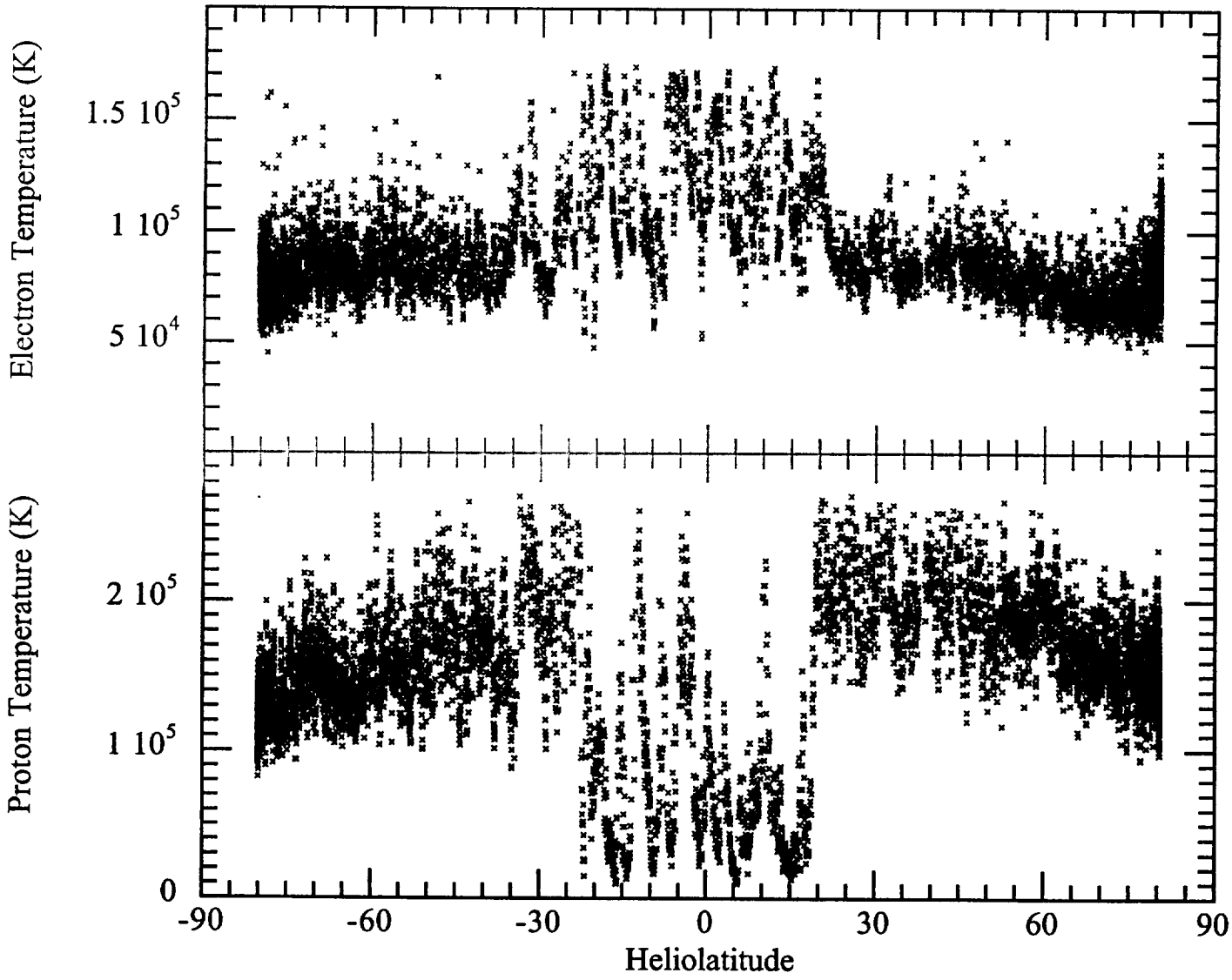

Figure 7
A Two-Fluid, MHD Coronal Model
Suess, Wang, Wu, Poletto, & McComas

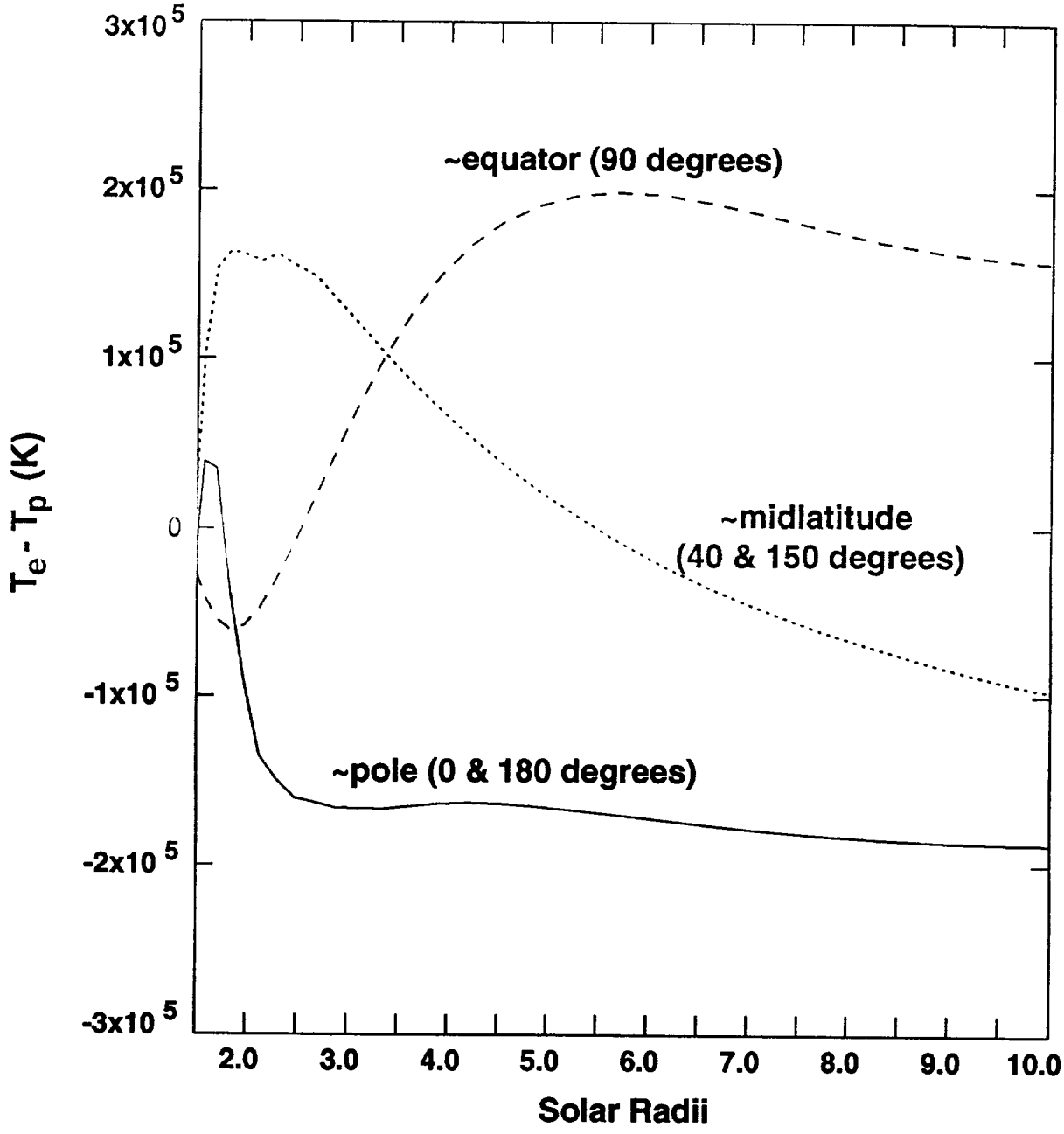

Figure 8
A Two-Fluid MHD Coronal Model
Suess, Wang, Wu, Poletto, & McComas